DOI: https://doi.org/10.21640/ns.v11i23.1665
Sección: Ciencias Naturales e Ingenierías

Estudio de remoción de arsénico (V) del agua mediante el uso de alúmina aglomerada

Study of arsenic (V) removal of water by using agglomerated alumina

Rafael Romero Toledo[1]
Víctor Ruiz Santoyo[2]
Luis M. Anaya Esparza[3]
Alejandro Pérez Larios[2]
Merced Martínez Rosales[1]

[1] Universidad de Guanajuato, División de Ciencias Naturales y Exactas, Departamento de Ingeniería Química
[2] Universidad de Guadalajara, Centro Universitario de Los Altos
[3] Universidad de Guadalajara, Centro Universitario de Los Altos, Departamento de Agricultura y Ciencias Agropecuarias

Autor para correspondencia: Rafael Romero Toledo, E-mail: r.romerotoledo@ugto.mx

Resumen

El arsénico es un elemento toxico para la salud humana. Persiste en el medio ambiente como resultado de la contaminación natural y antrópica, generando efectos nocivos para los consumidores. Algunos de ellos pueden se cáncer, trastornos cardiovasculares, hipertensión, enfermedad metabólica y neuropatía periférica. La adsorción se considera una de las tecnologías más eficaces ampliamente utilizadas en áreas de protección ambiental global. El objetivo de este estudio fue generar un adsorbente aglomerado de alúmina (A-1) de bajo costo para la eliminación efectiva de arsénico (V) del agua y su comparativo con una alúmina aglomerada comercial (A-2). Ambos de 5 mm de diámetro. Las propiedades de fisicoquímicas de los adsorbentes se caracterizaron mediante diversas técnicas, tales como: FRX, Potencial zeta, DRX, adsorción-desorción de N_2 y FE-SEM/EDS. Se realizaron experimentos por lotes para evaluar la eficiencia

de eliminación de As (V) en agua por A-1 y A-2. El punto de carga cero de A-1 y A-2 fue a pH 8.5 y 8.1, respectivamente. Los resultados experimentales en lotes indicaron que el aglomerado A-1 tiene una capacidad de adsorción mayor que A-2 (1.212 $mg \cdot g^{-1}$; 1.058 $mg \cdot g^{-1}$) en condiciones similares, concentración de 15 $mg \cdot L^{-1}$ of As (V), at 20 (±2) ºC y pH 7. El proceso de adsorción de As (V) en A-1 y A-2 siguió una cinética de seudoprimer orden y la isoterma de Freundlich. Los resultados demostraron que el aglomerado A-1 es un adsorbente atractivo para la eliminación efectiva de As (V) del agua.
Palabras clave: hidrólisis-precipitación; γ-alúmina; mesoporoso; As (V); tratamiento de agua

Abstract

Arsenic is a toxic element for human health. It persists in the environment as a result of natural and anthropic contamination, generating nocive effects for consumers. Some of them can be cancer, cardiovascular disorders, hypotension, metabolic disease and peripheral neuropathy. Adsorption is considered to be one of the most effective technologies widely used in global environmental protection areas. The objective of this study was to generate a low cost agglomerated alumina adsorbent (A-1) for the effective removal of arsenic (V) from water and its comparison with a commercial agglomerated alumina (A-2). Both of them of 5 mm of diameter. The physicochemical properties of the adsorbents were characterized by various techniques, such as: XRF, zeta potential, XRD, adsorption-desorption of N_2 and FE-SEM/EDS. Batch experiments were performed to evaluate the efficiency of removal of As (V) from water by A-1 and A-2. The point of zero charge of A-1 and A-2 was at pH 8.5 and 8.1, respectively. The experimental results in batches indicated that agglomerate A-1 has a higher adsorption capacity than A-2 (1.212 $mg \cdot g^{-1}$; 1.058 $mg \cdot g^{-1}$) in similar conditions, concentration of 15 $mg \cdot L^{-1}$ of As (V), temperature (20± 2 °C) and pH 7. The adsorption processes of As (V) in A-1 and A-2 followed the kinetics of Pseudo-first order kinetic and the Freundlich isotherm. The results showed that the agglomerate A-1 is an attractive adsorbent for the effective removal of As (V) from water.
Keywords: hydrolysis-precipitation; γ-alumina; mesoporous; As (V); water treatment

Recibido en: 06/09/2018

Aceptado en: 29/05/2019

Introduction

Arsenic is an ubiquitous element that ranks 20th in natural abundance. It comprises about 0.00005% of the earth's crust, 14th in the seawater, and 12th in the human body. It is a silver-grey brittle crystalline solid (Mohan & Pittman Jr., 2007) that is mobilized by natural weathering reactions, biological activity, geochemical reactions, volcanic emissions and other anthropogenic activities (Jeon *et al*., 2018).

Inorganic species of Arsenic (As) represent a potential threat to the environment, human health, and animal health due to their carcinogenic and many other nocive effects, as carcinogenic is after long-termor high-dose exposure. Additionally, it induces negative effects on the gastrointestinal tract and cardiac, vascular and central nervous systems (Sarkar & Paul, 2016; Yazdani *et al*., 2016) thus, pose a deleterious impact on public health. Due to the toxicological impacts of As and within order to reduce arsenic exposure through drinking water consumption, the United States Environmental Protection Agency (U.S. EPA), and the World Health Organization (WHO), have set the maximum acceptable As concentration for drinking water at 10 ppb (0.01 $mg \cdot L^{-1}$) (Dubey *et al*., 2017; Jeon *et al*., 2018). Nevertheless, the countries with exceeding As levels and limited monetary resources have retained the earlier WHO As concentration limit at 50 ppb (0.05 $mg \cdot L^{-1}$) (Yazdani *et al*., 2016), adopted for the Mexican legislation (Federación, 2000).

The presence of As in the environment arises from both natural and anthropogenic sources. The primary occurrence of As in groundwater results from the natural weathering of arsenic-containing rocks. Though in particular areas, high As concentrations may derive from industrial waste discharges and application of arsenical herbicides and pesticides (Yazdani *et al*., 2016; Song *et al*., 2015). The toxicity of As is governed by its speciation; the predominant As species in drinking water include the inorganic forms as arsenite (AsO_3^{3-}) and arsenate (AsO_4^{3-}). Arsenate [As (V)] is the dominant specie in natural surface water bodies and arsenite [As (III)]. It mainly exists in the groundwater (Komorowicz y Barałkiewicz, 2016). Arsenic (III) is usually more toxic than Arsenic (V); likewise, its removal from water is more difficult compared to As

(V). Generally, As (III) remains undissociated and is neutral and therefore, it only exhibits limited adsorption sites as compared to As (V) and an alternative to this situation is oxidizing As (III) to As (V) for its effective removal from water. Realizing such harmful effects of As on human health, there is a pressing need for exploring low-cost treatment technologies for As abatement (Shankar *et al*., 2014; Nicomel *et al*., 2015).

Several treatment methods have been developed for the removal of arsenic from water, including biological treatment (Caiyun *et al*., 2013), flotation (Taseidifar *et al*., 2017), nano-filtration (Saha & Sarkar, 2012), chemical precipitation (Li *et al*., 2011), coagulation (Pio *et al*., 2015), membrane process (Jeon *et al*., 2018), ion exchange (Yin *et al*., 2017), oxidation (Fontana *et al*., 2018), reverse osmosis or electrodialysis (Li *et al*., 2011) and adsorption process (Vieira *et al*., 2017). However, most methods for removing Arsenic have drawbacks, including high cost, lack of selectivity, low capacity, and difficulty in operation or regeneration. Some of them may produce large amounts of chemical sludge, which needs further treatment before being disposed. Among them, adsorption has been recognized as an effective and most extensive technique owing to its high removal efficiency, low cost as well as simple operation.

Adsorption is a commonly used technique for Arsenic removal from water. The effectiveness of adsorption techniques is greatly dependent on the physicochemical properties of the adsorptive materials. A large variety of adsorption materials have been tested for the removal of As from water, such as activated carbon, zeolite, metal oxide (Al, Fe, Ti, Mn, Cu, Zr and their composites), biosorbent, synthetic resin, industrial/agriculture byproducts or wastes (Caiyun *et al*., 2013; Yin *et al*., 2017). According to the classification stablished by the United Nations Environmental Program agency (UNEPA), activated alumina is one of the most available adsorbents for removing arsenic from contaminated water (Caiyun *et al*., 2013). Nevertheless, traditional commercial activated alumina (AA) generally suffers from the drawbacks of low adsorption capacity, slow adsorption rate and narrow working pH region, which should be closely associated with its ill-defined pore structure together with small surface area. However, their low adsorption capacities and poor adsorption kinetics still need improvements. An ideal adsorbent should have uniformly accessible pores, high surface area, and physical and chemical stability, due to that adsorption processes involve in the passage of the water through a contact bed where As V is removed by ion exchange or surface chemical reaction. In the past decades, mesoporous alumina (MA) has been synthesized employing different methods, where MA

exhibited an excellent performance in adsorption for many pollutants such as F-, Cr, Pb and Ni compared to AA.

Moreover, many researchers in most of their adsorption studies use powders for removal of As V.

In 2004, a study of As V removal using Mesoporous Alumina was reported obtaining a maximum adsorption capacity of 121 $mg \cdot g^{-1}$ (Younghun *et al*., 2004). On the other hand, Pradnya *et al*., made a modification to a mesoporous alumina with copper oxide, material that presented an adsorption capacity of 0.84 to 2.02 $mg \cdot g^{-1}$ for As V (Pradnya *et al*., 2011). Caiyung *et al*., reports the maximum adsorption capacity of As V is 36.6 $mg \cdot g^{-1}$, at almost neutral pH (6.6 ± 0.1). The above using a mesoporous alumina, synthesized by combining the three-block copolymer Pluronic P123 as a template (Caiyun *et al*., 2013). Another study in 2018 revealed a maximum As V removal capacity of about 93.06% of an initial As V concentration of 0.5 $mg \cdot L^{-1}$ using Activated Alumina (Majumder, 2018). A recent study reports the adsorption capacity of a mesoporous alumina of 90 $mg \cdot g^{-1}$ and a commercial alumina of 54 $mg \cdot g^{-1}$ of As V (Inchaurrondo *et al*., 2019).

The results obtained in the previous studies are very attractive, however, in the face of the real problems of society, needs arise at the industrial level, where the dust presents disadvantages, such as: it is dragged by the flow of water, it is directly affected by the pH breaking the structure of the particles, it presents obstruction due to the generation of a mixture, the filters at industrial level present large flows, where the powders go from being an adsorbent to a pollutant. Due to the above, it was decided to study the adsorption of As (V) in agglomerates of 5 mm of diameter, material that do not has disadvantages in packed adsorption columns of industrial level.

The main objective of this research was to investigate the efficiency of two agglomerated adsorbents (synthesized (low cost) and commercial alumina of 5 mm of diameter) in the removal of arsenic V from water at variable pH levels (5 and 7), as well as the arsenic adsorption behavior under different water quality conditions.

Materials and methods

Chemicals: Hidrated aluminum sulfate ($Al_2(SO_4)_3 \cdot H_2O$) with purity of 95% (wt.), technical-grade (TG), Alfa-Omega, S.A. of low cost, distilled water (Karal S.A. of C.V), Nitric acid (HNO_3, karal 70%), Hexane (C_6H_{14}, J. T. Baker 99.8%), Ammonium hydroxide (NH_4OH, Karal 30%) and ammonia gas anhydrous (NH_3, Praxair 99.98%) The above mentioned were the starting materials to obtain agglomerate alumina. Deionized water (Karal S.A. of C.V), Sodium arsenate dibasic heptahydrate ($HAsNa_2O_4 \cdot 7H_2O$, Sigma-Aldrich 98%) as As V. Commercial activated alumina (Al_2O_3) of 5 mm diameter were used as comparison material (Alquimia Mexicana S. de R.L.).

Synthesis and agglomeration: Fig. 1 shows the diagram of the process used in this research for obtaining the adsorbent. This methodology consists of five steps. In the first step, the $Al_2(SO_4)_3 \cdot H_2O$ was dissolved into distilled water, after that the saturated solution of $Al_2(SO_4)_3 \cdot H_2O$ was filtered for removal of insoluble impurities. In the second step, precursor were prepared by dropping saturated solution of $Al_2(SO_4)_3 \cdot H_2O$ into a solution of water and ammonia gas, under rigorous magnetic stirring, at temperature of 70 ºC. In the third step, the precipitated solution was filtered; the precipitated of pseudoboehmite was rinsed with distilled water three times respectively and then dried at 110 °C for 12 h. In the fourth step, the agglomeration of pseudoboehmite in solid spheres was through using a colloidal solution, prepared using pseudoboehmite, nitric acid, distilled water. A glass column with 30 mL of hexane and 250 mL of ammonium hydroxide for the agglomeration of colloidal solution by dripping was used (Trejo & Bonilla, 2004). Finally, the fifth step, the activation and/or phase change of the agglomerates of pseudoboehmite to γ-alumina was performed by thermal treatment at 500 °C for 4 h (Renuka, Shijina & Praveen, 2012).

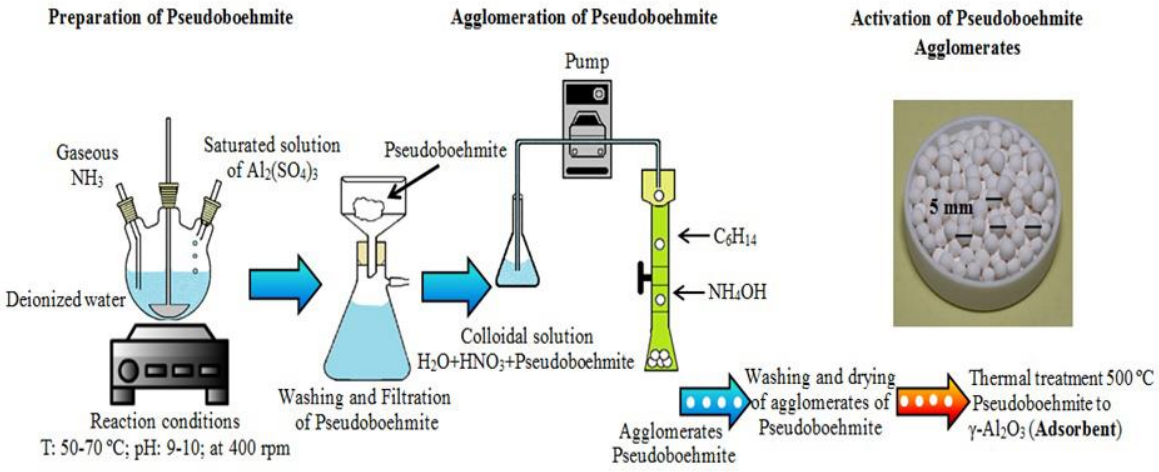

Fig. 1. Diagram of adsorbent preparation process.

Batch adsorption experiments: The solutions of As (V) were obtained by dissolving in deionized water the arsenate dibasic sodium heptahydrate ($HAsNa_2O_4{\cdot}7H_2O$). The tests were carried out in a batch reactor with magnetic stirring at 1000 rpm. The temperature of the system was controlled with an external heater-cooler. For the determination of arsenic concentrations, an Agilent Technologies Model 4100 MP-AES plasma atomic emission spectrometer was used. The adsorption capacity q ($mg{\cdot}g^{-1}$) was calculated using the following equation:

$$q_e = \frac{(C_o - C_e)V}{m} \qquad (1)$$

Where q_e is the adsorption capacity ($mg{\cdot}g^{-1}$), C_o is the concentration before adsorption ($mg{\cdot}L^{-1}$), C_e is the concentration after adsorption ($mg{\cdot}L^{-1}$), V is the volume of the solution (L) and m is the mass of the adsorbent (g) (Li *et al*., 2013). The adsorption kinetics were performed at an initial arsenic concentration of 15 $mg{\cdot}L^{-1}$ to 20 (± 2) ° C and pH 7 ± 0.2 (pH 6 to 8.5, range of groundwater), the adsorbent dose used was 250 $mg{\cdot}L^{-1}$ (0.25 g of adsorbent in 100 mL of solution), arsenic measurements were made at different adsorption times up to 240 min.

For the effect of pH of the initial solution of As (V) the tests were performed only for sample A-1, with a dose of adsorbent of 250 $mg{\cdot}L^{-1}$ and an initial concentration of As (V) of 25 $mg{\cdot}L^{-1}$ at a T = 20 (± 2) °C. The initial pH of the solutions was adjusted using NaOH and HCl 0.1M in a pH range of 4 to 9.

The adsorption isotherms was performed at 20 (± 2) ° C and at the original pH of each solution (6.7 ± 0.5) using, a range of 1 to 25 $mg \cdot L^{-1}$ of As (V) concentration. The equilibrium time of each of the adsorbent materials was used. The adsorbent dose was 250 $mg \cdot L^{-1}$. The adsorption kinetics and isotherms adsorption was determined by nonlinear regression analysis through the Statistical graphics software.

Physicochemical characterization of adsorbents

N_2 physisorption: Textural properties were characterized by N_2 adsorption (Micromeritics, ASAP 2010). The samples were degassed at 200 ºC for 3 h, under vacuum. Nitrogen adsorption isotherms were measured at liquid N_2 temperature (77 K), and N_2 pressures ranging from 10^{-6} to 1.0 P/P_0. Surface area was calculated according to Brunauer–Emmett–Teller (BET) method and the pore size distribution was obtained according to the Barret–Joyner–Halenda (BJH) method.

X-ray diffraction (XRD): The crystalline properties of the samples were determined at room temperature by using X-ray powder diffraction. A siemens D-500 diffractometer, equipped with a CuKα radiation anode, was used for these measurements, under the following conditions: sweep of 10-80º at an angle 2θ, with wavelength k = 1.54 Å, with applied voltage of 30 kV and current of 20 mA.

Zeta potential analysis (pZ): The agglomerates of alumina and commercial alumina were crushed and dispersed in water. They were measured by electroacoustic technique with a particle size analyzer (AcoustoSizer II, ESA; Colloidal Dynamics, USA), in a pH range of 4 to 9.5, where the pH was adjusted with NaOH and HCl at 0.1M.

Field-emission scanning electron microscopy (FE-SEM): The surface morphology was examined using JEOL JSM 7600-F Field-Emission. It was equipped with energy dispersive X-ray spectrometer (EDS) for the determination of the chemical composition.

XRF analysis: The chemical composition was performed on a Rigaku NEX CG X-ray Fluorescence Spectrometer using energy dispersion (EDXRF). The spectrometer has a Pd anode

X-ray tube, maximum power of 50W with maximum voltage of 50kV, current of -2 mA and He atmosphere.

Results and discussion

X-ray fluorescence (XRF) analysis

The results of semi-quantitative analysis of XRF are shown in Table 1. In Table 1 the weight percentage (wt. %) of the chemical composition of alumina agglomerates can be observed. It is evident that there is Al and O in a major percentage, it corresponds to the general structural formula of the alumina (Al_2O_3) with some other minor constituents such as Si, S, Ca and Fe, attributed to impurities and residues of the synthesis process corresponding to the adsorbent A-1. On the other hand, the adsorbent A-2 presented Al and O in greater quantity with some other minor constituents such as Si, S, Ca, K, Fe and Zn in wt. % are attributed to impurities in the structure, being Si and Ca those of greater proportions. The results presented in Table 1 for A-1 adsorbent are of the fluorescence analysis after filtering the solution of aluminum sulfate to remove unsolvable impurities. In addition, it was determined that the unsolvable impurities retained in the filter are around of 5 wt. %.

Table 1. The chemical composition of A-1 and A-2 (wt. %), determined by X-ray fluorescence.

Precursor	unsolvable	Al	Si	S	Ca	K	Fe	Zn	O
A-1	5%	45.3	0.032	0.464	0.048	-	0.063	-	54.1
A-2	-	44.4	0.38	0.009	0.206	0.011	0.017	0.0003	54.8

Zeta potential measurement

The oxidation state of As and its mobility are mainly controlled by redox conditions (Eh) and pH (Fig. 2). In aqueous systems, the As is found, as a dissolved species, forming oxyanions. The As (III) is found as H_3AsO_3 and its corresponding dissociation products ($H_4AsO_3^+$, H_2AsO^{-3}, $HAsO_3^{-2}$ and AsO_3^{-3}), which, under oxidizing conditions, are dominant at alkaline pH. However, the form without charge of As (III) [$As(OH)_3$] is dominant in reduced and anoxic environments, being thus the most toxic and difficult to eliminate. On the other hand, the As (V) is present in the form H_3AsO_4 and its corresponding dissociation products ($H_2AsO_4^-$, $HAsO_4^{-2}$ and AsO_4^{-3}), being dominant under oxidizing conditions at acid pH in aqueous and aerobic environments as shown in Fig. 2 (Akter *et al*., 2005).

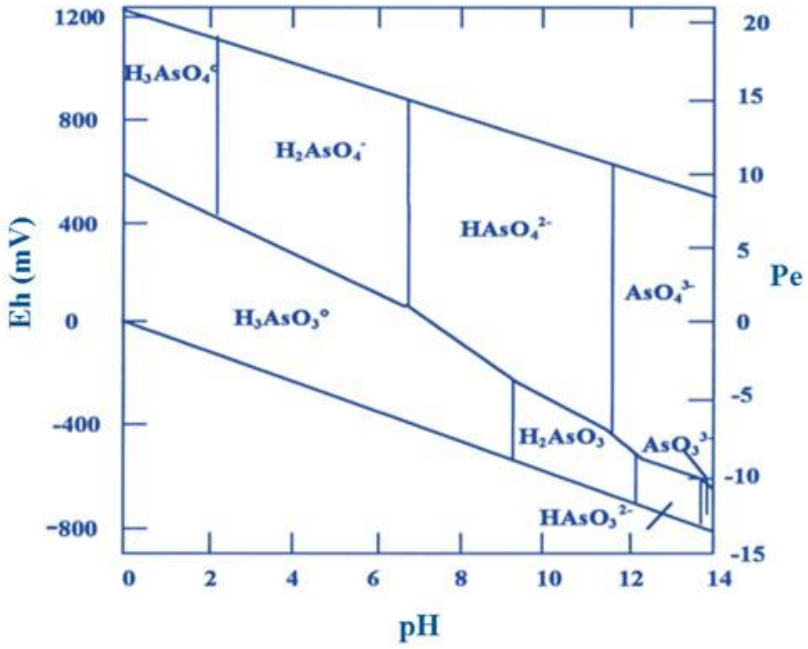

Fig. 2. Redox potential (Eh)–pH diagram for aqueous arsenic species in the system As-O_2-H_2O at 25 °C and 1 bar total pressure, (Smedley and Kinniburgh, 2002).

The pH of the solution may affect both the chemical environment of the surface of the adsorbents and the As (V) species. In this sense, the zeta potential analysis was performed for agglomerates

A-1 and A-2. In addition, the effect of the pH of the initial solution of As (V) on the adsorbent A-1 was investigated. Fig. 3 shows the analyzed zeta potential profiles of agglomerates A-1 and A-2 versus pH. In the present work, as the pH increased from 4.5 to 9.4, the zeta potential of agglomerate A-1 steadily decreased from 33 to −24 mV, and the point of zero charge (pzc) for this agglomerate adsorbent was around 8.5, this result corresponds to the observed and analyzed in Fig. 2. The zeta potential of agglomerate A-2 steadily decreased from 30 to −25 mV, and the point of zero charge (pzc) was around 8.1, which are close to those values reported in the literature (e.g., 8.0, 8.5–9.3) (Liang *et al*., 2017; Jiemin *et al*., 2014; Zamorategui *et al*., 2016), with the relative difference being smaller than 10%.

The stability of the suspensions of the agglomerated adsorbents studied by means of zeta potential at different pH is shown in Fig. 3(a). The agglomerates particles have an important dependence with pH, giving positive zeta potentials at acidic pH and negative ones at basic pH for both agglomerates. For values of pH >8.5 both A-1 and A-2 have a negative charge and for lower pH the particles have opposite charge.

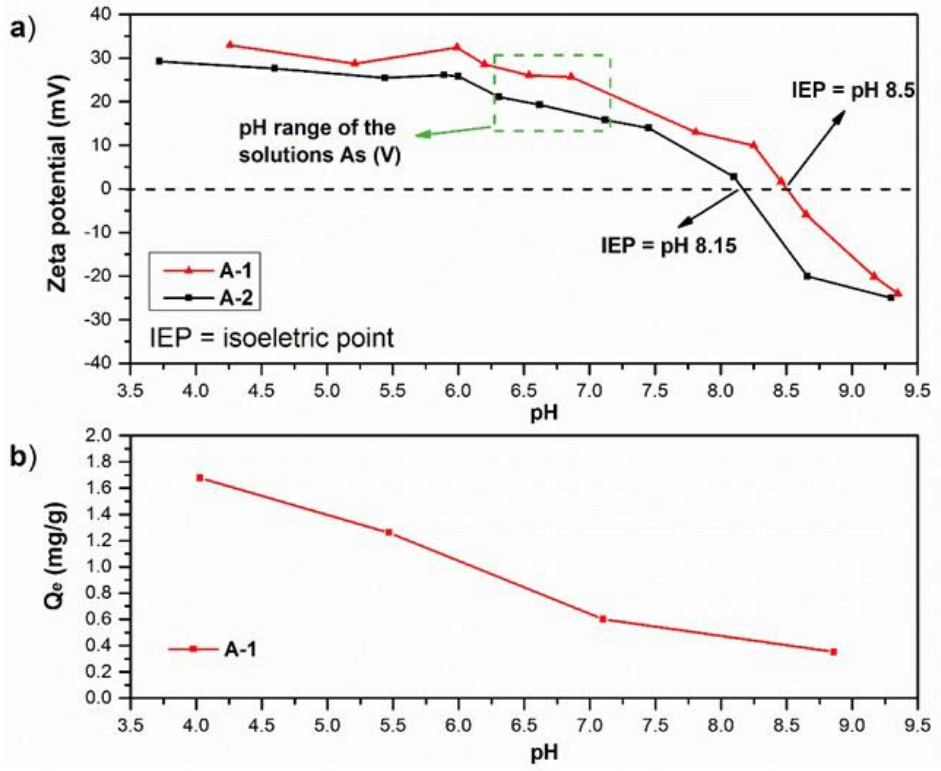

Fig. 3. a) Zeta potential of the A-1 and A-2 at different pH values, T = 20 ºC and b) effect of pH of the initial solution of As (V) on the A-1.

It was observed that the adsorption capacity decreased as the potential of the surface of the adsorbent A-1 decreased because the positive surface charge was more attractive for the negative species of As (V). When the pH value exceeded the pH value 8.1 and pH 8.5 for A-2 and A-1 respectively of the isoelectric point, the surface sites are negatively charged causing a considerable decrease in the value of the adsorption capacity due to the electrostatic repulsive effect, as seen in Fig. 2(b).

X-ray diffraction (XRD) analysis

Fig. 4 shows the wide-angle XRD (WAXRD) patterns of the agglomerates A-1 and A-2. The X-ray diffraction pattern was performed of 10 – 80º at an angle 2θ. The results of the WAXRD patterns show seven weak diffraction peaks for the agglomerate A-1. They are observed at 2θ= 19.2, 31.0, 36.6, 39.3, 46, 61.5, and 67º, which can be indexed as the (111), (220), (311), (222), (400), (511), and (440) reflections of γ-alumina (JCPDS card 10-0425) (Leyva *et al*., 2008; Yuan *et al*., 2013; Asuha *et al*., 2018), indicating that the adsorbent A-1 is mainly composed of γ-Al_2O_3. Therefore, it revealed that the agglomerate A-1 presents a low degree of crystallinity and that it has a bimodal porous with an amorphous wall according to the literature (Leyva *et al*., 2008). The characteristic peaks of the agglomerate A-2 are attributed to the aluminum oxyhydroxide (γ-AlOOH) phase and are observed at 2θ= 15.2, 27.5, 38.0, 48.0, 56.0, 64.0 and 72.5º, which can be indexed as the (020), (021), (130), (002), (151), (200) and (152), according to (JCPDS Card No. 21-1307) (Choi *et al*., 2017). However, one peak is observed about 2θ = 43° for A-2 that does not corresponds to the γ-AlOOH and/or γ-alumina phases, which is attributed to a shift of peaks in the structure. The above mentioned, attributing that the commercial agglomerate A-2 is a mixture of γ-alumina and/or boehmite phase the latter in greater quantity, because it presents alumina peaks about of 19º, 39º and 67º in 2 theta.

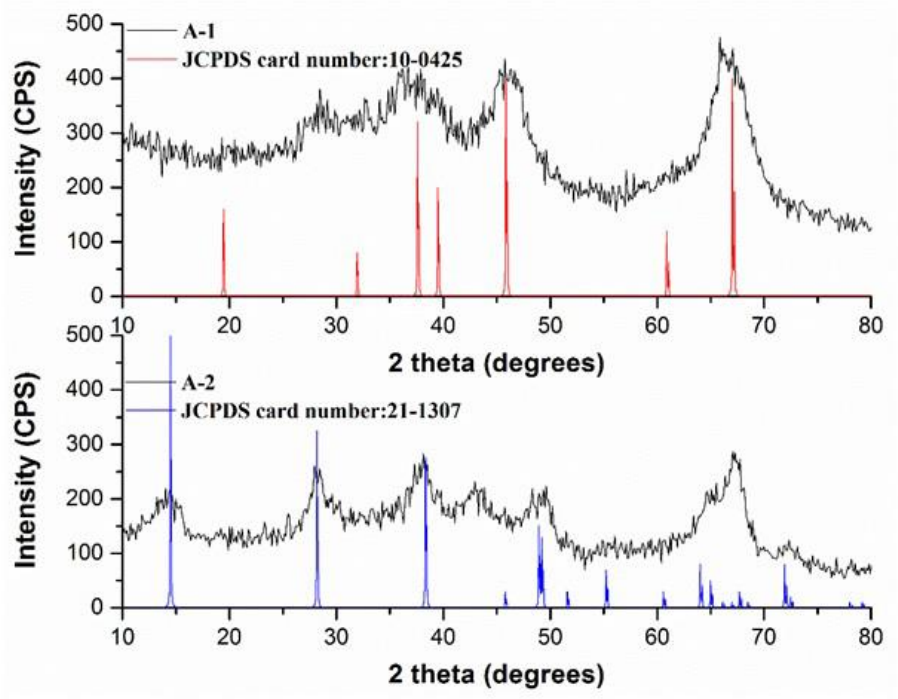

Fig. 4. XRD patterns of A-1 and A-2, JCPDS Cards number: boehmite (21-1307), γ-Al_2O_3 (10-0425).

Textural properties

N_2 adsorption–desorption isotherms and Barrett–Joyner–Halenda (BJH) pore size distribution curve of agglomerates A-1 and A-2, are shows in Fig. 5. According to the results of N_2 adsorption–desorption isotherms, both agglomerates present type IV isotherms (IUPAC classification) (Kenneth & Ruth, 2004; Sing *et al*., 1985), as see in Fig. 5(a). Two well-distinguished regions in the adsorption isotherms are evident: (i) monolayer–multilayer adsorption and (ii) capillary condensation (Caiyun *et al*., 2013). The first increase in adsorption at relative pressure P/P0 < 0.2 is due to multilayer adsorption on the surface while the second increase at P/P0 = 0.42–0.97 arises from capillary condensation in the mesoporous with nitrogen multilayers adsorbed on the inner surface (Caiyun *et al*., 2013; Zhang *et al*., 2016). The major consumption of N_2 in the adsorption-desorption isotherm of agglomerate A-2 occurred at a low

relative more pressure that the agglomerate A-1 and reached a plateau at high relative pressure. In agreement with the results obtained, the pore size distribution for both adsorbents agglomerates are micro and mesoporous materials respectively, Fig. 5b. These agglomerated adsorbents presented a different distribution of pores ranging from 2 to about 100 nm, centered at 5.0 and 3.5 for A-1 and A-2, respectively, exhibiting the agglomerate A-1a major pore homogeneity. But also, the sample A-1 exhibits a large surface area of 272 m^2g^{-1} and a pore volume of 0.86 cm^3g^{-1}. On other hand, the agglomerate A-2 exhibits a surface area of 206 m^2g^{-1} and a pore volume of 0.39 cm^3g^{-1}. The difference of the textural values can be attributed to a higher content of metals as impurity in the agglomerate A-2, as shown in the XRF analysis (Table 1) and a high index of crystallinity, as observed in the diffraction pattern, Fig. 4.

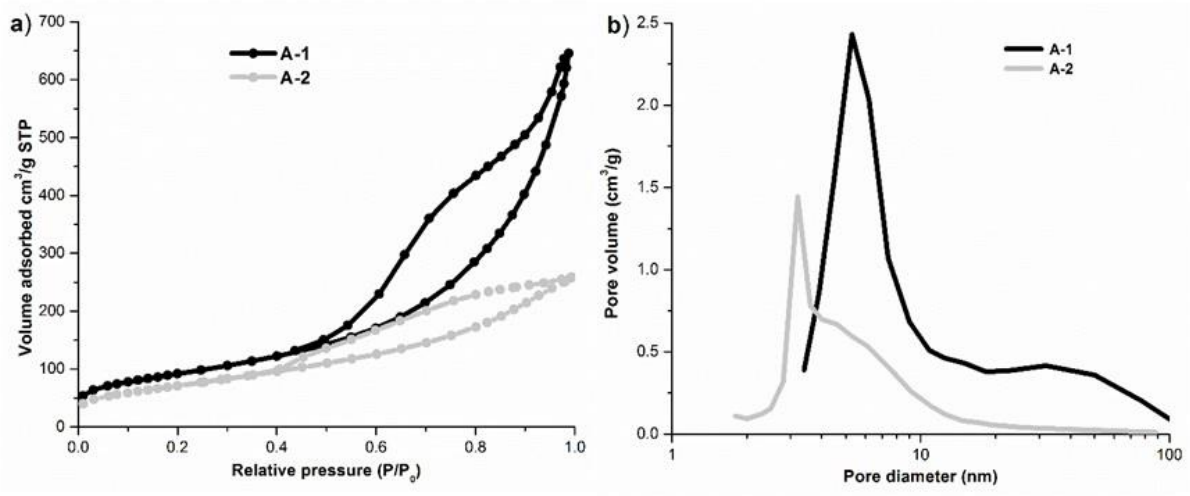

Fig. 5. a) N_2 adsorption–desorption isotherms and b) pore size distribution curves of the agglomerates A-1 and A-2.

Field-Emission scanning electron microscopy (FE-SEM)

The detailed morphology and internal structure of the agglomerates A-1 and A-2 was then investigated by field emission scanning electron microscopy (FESEM), which is shown in Fig.

6a-b. The FESEM images before adsorption showed morphology differences between adsorbents. The micrographs consists of nano-fibers that tend to form amorphous agglomerates due to their high surface energy, therefore generating high porosity showing attractive potential for adsorption of As (V). In comparison with the morphology of the agglomerate A-2, Fig. 6(b), we can see that it exhibits a higher degree of agglomeration in the surface and consequently has a lot of small pores. For the agglomerate A-1, the pores are of wormhole channel-sponge like motif, hinting to a highly interconnected porous system, observing a greater porosity and pore homogeneity, as determined by the BET analysis**.** This kind of interconnected pores is believed to be useful for catalytic and/or adsorption applications from a diffusion point of view (Renuka, Shijina & Praveen, 2012).

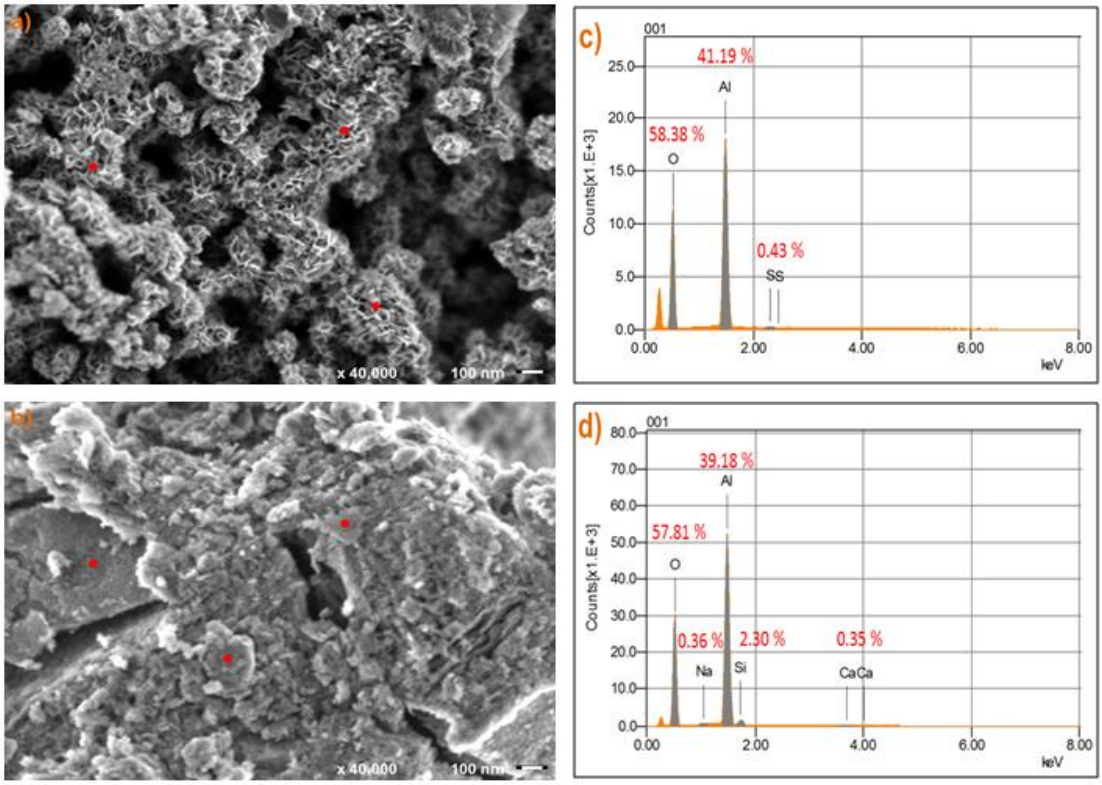

Fig. 6. FE-SEM image of agglomerates alumina before As (V) adsorption and Average of EDS analysis (a, c) A-1, (b, d) A-2.

The FE-SEM images of A-1 and A-2, Fig. 6(a, b) show the points of places where the electron beam for determining elemental EDS analysis were set. The average chemical compositions of the material surfaces determined using EDS analysis were summarized in Fig. 6(c, d).

The energy dispersive X-ray analysis reveals the existence of Al, O and S, further confirming the general structure of the alumina formula for A-1. The EDS data showed compositional differences between the adsorbent A-1 and A-2. The energy dispersive X-ray analysis confirmed the presence of Al, O, Ca and Si, in the structure of the agglomerate adsorbent A-2. On the other hand, the absence of some contaminants in both samples is observed from the EDS analysis, as was determined by XRF analysis. This is attributed to a homogenously distributed in the matrix and the limit is expressed as an atomic fraction.

Batch adsorption of As (V) on A-1 and A-2

Adsorption kinetics study

Fig. 7 shows the adsorption kinetic study data of As (V) on A-1 and A-2 at pH 7.0 and the best-fit model curves. The amount of As (V) adsorbed by A-2 increased slowly over a period of 3.5 h. On the other hand, As (V) adsorption by A-1 occurred more rapidly and reached equilibrium within about 2.5 h. Others authors reported that the adsorption of As (V) in Mesoporous Alumina was found to be time-dependent and the adsorption was rapid in the first 5 h and then slowed notably as the reaction approached equilibrium (Younghun *et al*., 2004).

The experimental data obtained from the adsorption kinetics of As (V) of A-1 and A-2 were analyzed using the kinetic models of Pseudo-first-order [Eq. (2)], Pseudo-second order [Eq. (3)] (Basu, Gupta & Ghosh, 2012; D'Arcy *et al*., 2011) and Elovich [Eq. (4)] (Li *et al*., 2013) and were applied to fit the adsorption kinetic study data in Fig. 6.

Pseudo-first-order $$q_t = q_e * (1 - e^{K_1 * t}) \quad (2)$$

Pseudo-second-order $$q_t = \frac{(q_e^2 * K_2 * t)}{(1 + t * K_2 * q_e)} \quad (3)$$

Elovich $$q_t = \frac{1}{\beta} * ln(1 + \alpha * \beta \quad (4)$$

Where K_1 (min^{-1}) and K_2 ($g \cdot mg^{-1} \cdot min^{-1}$) are the velocity constant of the pseudo-first-order and pseudo-second-order respectively; α ($mg \cdot g^{-1} \cdot min^{-1}$) is the initial rate of adsorption and β ($g \cdot mg^{-1}$) is the sign of desorption of the Elovich model; q_t ($mg \cdot g^{-1}$) and q_e ($mg \cdot g^{-1}$) are the adsorption capacities at time t and at equilibrium, respectively (Basu, Gupta & Ghosh, 2012; D'Arcy *et al*., 2011; Li *et al*., 2013). In the case of the Pseudo-second-order model h, the initial adsorption velocity is considered (D'Arcy *et al*., 2011):

$$h = K_2 q_e^2 \quad (5)$$

The best-fit parameters for the pseudo-first-order model, pseudo-second-order model and Elovich model are presented in Table 2. The R^2 values of the pseudo-first-order model were higher than those of the pseudo-second-order model and Elovich model, which revealed that the As (V) adsorption on A-1 followed the pseudo-first-order kinetics. In the case of the synthesized adsorbent A-2, there was not considerable difference between the three models compared. There is much higher rate constant k_1 for A-1 (0.013) than for A-2 (0.005). It also indicated the fastest adsorption kinetics of As (V) on A-1 than on A-2.

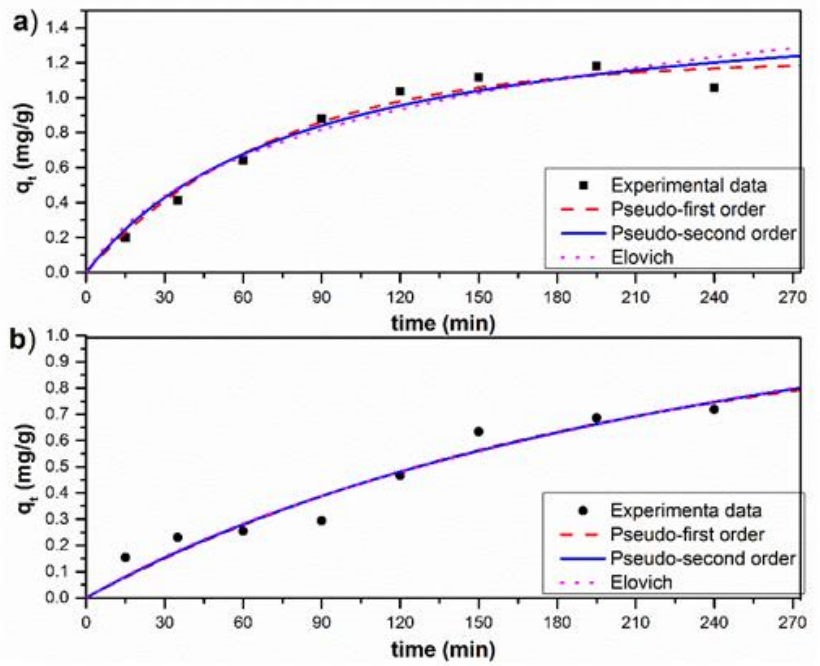

Fig. 7. Plots q_t (mg·g-1) versus contact time (min), and no-linear fits of date with Pseudo-first order, Pseudo-second order and Elovich models with a) A-1 and b) A-2.

In most cases, the pseudo-first-order equation does not fit well for the whole range of contact time and it is generally applicable over the initial 30 min of the sorption process (Ho, 2006; Erden, Kaymaz & Pazarlioglu, 2011). As (V) is adsorbed on metal oxides and hydroxides through bonding interactions onto mineral surfaces sites (Jung *et al*., 2014). The rapid adsorption of As (V) on the adsorbent A-1 within the first 2.5 h (Fig. 7) could be mainly attributed to the specific adsorption of the As (V) on the A-1 surface because it was readily accessible to As (V) and internal surface sites due to the larger volume and pore diameter. The slower adsorption was ascribed to slow diffusion of As (V) into the pores of the A-2 due to little accessibility to pores and the internal surface area.

Table 2. Parameters of the kinetic models of Pseudo-first order, Pseudo second order and Elovich in the adsorption of As (V).

Kinetic model	**Adsorbents**	
	A-1	A-2
Pseudo-first order model		
qe ($mg \cdot g^{-1}$)	1.212	1.058
K_1 (min^{-1})	0.013	0.005
R^2	0.970	0.930
Pseudo-second order model		
qe (mg·g)	1.618	1.676
K_2 ($g \cdot mg^{-1} \cdot min^{-1}$)	0.007	0.002
h ($mg \cdot g^{-1} \cdot min^{-1}$)	0.019	0.005
R^2	0.950	0.930
Elovich model		
α ($mg \cdot g^{-1} \cdot min^{-1}$)	0.023	0.005
β ($g \cdot mg^{-1}$)	2.077	1.582
R^2	0.928	0.930

Adsorption isotherms

The adsorption isotherms describe the interaction between adsorbate molecules and adsorbent, which are important for understanding the adsorption mechanism. In order to determine and compare the adsorption capacities, the Langmuir and Freundlich isotherm equations were used to fit the experimental data for As (V) adsorption on agglomerates A-2 and A-1, respectively. The modeled adsorption isotherm is an invaluable non-linear curve describing the adsorption phenomenon at a constant temperature and pH. The mathematical correlation that is depicted by the modeling analysis is important for operational design and for applicable practice of the adsorption systems (Xunjun, 2015). The Langmuir model describes quantitatively the formation of an adsorbate monolayer on the outer surface of the adsorbent (Marshahida & Erma, 2016). The Langmuir isotherm is valid for the adsorption of a monolayer on a surface containing a finite number of identical sites. The model assumes uniform adsorption energies (Langmuir, 1916; Marshahida & Erma, 2016). Based on these considerations, the model is represented by the [Eq. (6)]:

$$q_e = \frac{q_{max}\, K_L\, C_e}{1 + K_L\, C_e} \qquad (6)$$

Where Ce is the concentration of adsorbate at equilibrium ($mg \cdot L^{-1}$), qe is the adsorption capacity at equilibrium per gram of adsorbent ($mg \cdot g^{-1}$), qmax is the maximum capacity of coating adsorption of a monolayer $(mg \cdot g)^{-1}$), K_L is the Langmuir constant related to the adsorption energy ($L \cdot mg^{-1}$) (Hongmei *et al*., 2014).

Freundlich model is based on the hypothesis that only physisorption (formation of multilayers) intervenes and that there is no association of molecules after its adsorption (Freundlich, 1906). This model has the limitation of not admitting saturation phenomena. Based on these considerations, the model is represented by the [Eq. (7)]:

$$q_e = K_f C_e^{1/n} \qquad (7)$$

Where Ce is the concentration of adsorbate at equilibrium (mg L^{-1}), q_e is the adsorption capacity at equilibrium per gram of adsorbent (mg g^{-1}), K_f is a relative capacity of adsorption (mg g^{-1}), n is an affinity constant and 1/n represents an indication of the intensity of adsorption (Hongmei *et al*., 2014; Marshahida & Erma, 2016).

Fig. 8 illustrated the adsorption isotherms of As (V) on the A-1 and A-2 at pH 7.0. The A-1 agglomerate slightly increased the amount of As (V) adsorbed. The best-fit parameters are listed in Table 3. The R^2 values suggested that the Freundlich isotherm described the adsorption data better than the Langmuir isotherm. The qmax value for A-1 was 1.25 mg·g^{-1}, the agglomerate A-2 has much lower qmax (0.68 mg·g^{-1}) than A-1.

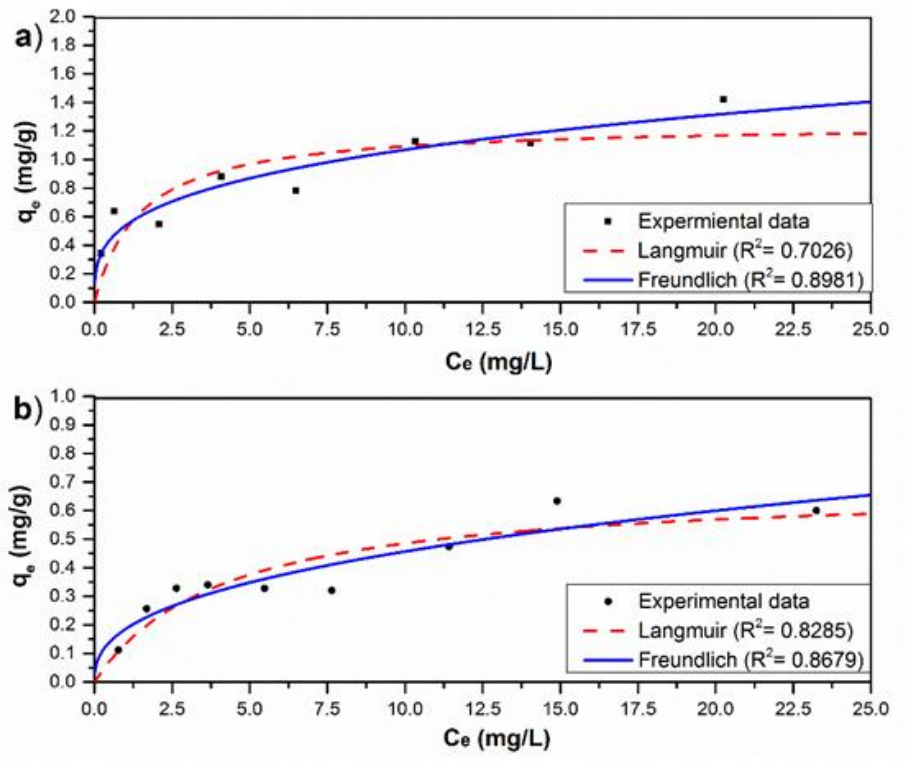

Fig. 8. Plots of equilibrium adsorption data on As (V) removal at pH = 6.7 (±0.5) and T=20(±2) °C, and no-linear fits of date with Langmuir and Freundlich model equations with a) A-1 and b) A-2.

The model of best-fit in both materials was the Freundlich model that indicates a physisorption (formation of multilayers) and that there is no association of molecules after their adsorption. The

values of the relative capacity of adsorption (Kf) and of the adsorption intensity (1/n) obtained were 0.5370 $mg \cdot g^{-1}$ and 0.2987 for the adsorbent A-1; of 0.1851 $mg \cdot g^{-1}$ and 0.3925 for the adsorbent A-2, respectively.

The mechanisms of removal of the species of As (V) could be related with two factors: (i) the electrostatic charges. According to the obtained results of potential z and the effect of the initial pH (shown in Fig. 2) to a lower pH a greater capacity of adsorption was obtained. The surface of the adsorbent remained positively charged, and as the pH of the solution was increased, the positive potential of the surface decreased. It was also observed with the adsorption capacity, with a minimum value of removal to the value of pH where the surface was negatively charged. (ii) It may be presenting an adsorption mechanism due to the OH groups on the surface of the adsorbent, this can be attributed to the adsorbent A-1 presented a capacity of adsorption of 0.352 $mg \cdot g^{-1}$ at pH 8.86 with its negatively charged surface and only negative As (V) species being found (Sreejesh *et al*., 2014; Mohan & Pittman, 2007).

Likewise, it was observed that in the pH range those adsorption isotherms of the two adsorbents were made. The agglomerate A-1 presents a greater potential (positive charge) on the surface, which could have been an important factor for the greater adsorption capacity with respect to agglomerate A-2.

Table 3. Parameters of the models of the Langmuir and Freundlich isotherms in the adsorption of As (V).

	Adsorbents	
	A-1	A-2
Langmuir model		
q_{max} $(mg \cdot g^{-1})$	1.253	0.686
$K_L (L \cdot mg^{-1})$	0.680	0.241
R^2	0.702	0.828
Freundlich model		
$K_f (mg \cdot g^{-1})$	0.537	0.185
n	3.348	2.547
1/n	0.298	0.392
R^2	0.898	0.867

Conclusion

It was possible to obtain an alumina with mesoporous structure A-1 from low cost aluminum sulphate, synthesized by the hydrolysis / precipitation method. The powder was agglomerated by a colloidal suspension with good properties as an adsorbent effective material, which can be used to remove the As V present in drinking water. The A-1 agglomerates have higher zeta potential and adsorption capacity compared to A-2 agglomerate at the same pH, attributed to ill-defined pore structures and crystalline. The adsorption behavior of A-1 and A-2 was described well with the pseudo-firts-order kinetics and the adsorption isotherms were described with the Freundlich equation. The maximum adsorption capacities of A-1 and A-2 determined by the Langmuir equation were 1.25 and 0.68 $mg \cdot g^{-1}$ at pH = 7.0, respectively. This is highly attractive for elimination of As (V) at industrial level in maximum concentrations of 1.3 $mg \cdot L^{-1}$, without presenting disadvantages compared with powders to achieve the permissible limits adopted by the Mexican legislation.

Acknowledgements

Authors gratefully acknowledge the support by the National Council on Science and Technology (Conacyt) and University of Guanajuato, México.

Referencias

Akter Farzana Kazi, Owens Gary, Davey E. David, and Naidu Ravi. (2005). Arsenic Speciation and Toxicity in Biological Systems. Reviews of Environmental Contamination and Toxicology, 184, 97–149.

Asuha, S., Talintuya T., Han, Y., and Zhao, S. (2018). Selective extraction of aluminum from coal-bearing kaolinite by room-temperature mechanochemical method for the preparation of γ-Al_2O_3 powder. Powder Technology, 325: 121-125.

Caiyun Han, Hongping Pu, Hongying Li, Lian Deng, Si Huang, Sufang He, Yongming Luo. (2013). The optimization of As (V) removal over mesoporous alumina by using response surface methodology and adsorption mechanism. Journal of Hazardous Materials, 254–255, 301–309.

Choi, J., Yoo, K. S., Kim, S. D., Park, H. K., Nam, C. W., and Kim, J. (2017). Synthesis of mesoporous spherical γ-Al_2O_3 particles with varying porosity by spray pyrolysis of commercial boehmite. Journal of Industrial and Engineering Chemistry, 56: 151-156.

Dubey, S. P., Dwivedi, A. D., Sillanpää, M., Lee, H., Kwon, Y. N., & Lee, C. (2017). Adsorption of As (V) by boehmite and alumina of different morphologies prepared under hydrothermal conditions. Chemosphere, 169, 99-106.

Erden Emre, Kaymaz Yasin, Pazarlioglu Kasikara Nurdan. (2011). Biosorption kinetics of a direct azo dye Sirius Blue K-CFN by Trametes versicolor. Electronic Journal of Biotechnology, Vol 14, No. 2.

Federación, D. O. (2000). Modificación a la norma oficial Mexicana NOM-127-SSA1-1994. Salud ambiental, agua para uso y consumo humano. Límites permisibles de calidad y tratamientos a que debe someterse el agua para su potabilización", octubre, 20, 1-8.

Fontana, K. B., Lenzi, G. G., Seára, E. C. R., and Chaves, S. E. (2018). Comparision of photocatalysis and photolysis processes for arsenic oxidation in water. Ecotoxicology and Environmental Safety. 151: 127-131.

Freundlich, H.M.F. (1906). Over the adsorption in solution. The Journal of Physical Chemistry, Vol. 57, pp. 385-471.

Hongmei Jin, Sergio Capareda, Zhizhou Chang, Jun Gao, Yueding Xu, Jianying Zhang. (2014). Biochar pyrolytically produced from municipal solid wastes for aqueous As(V) removal: Adsorption property and its improvement with KOH activation. Bioresource Technology, 169, 622–629.

Jeon, E. K., Ryu, S., Park, S. W., Wang, L., Tsang, D. C. W., and Baek, K. (2018). Enhanced adsorption of arsenic onto alum sludge modified by calcination. Journal of Cleaner Production 176: 54-62.

Jiemin Cheng, Xiaoguang Meng, Chuanyong Jing, Jumin Hao. (2014). La^{3+}-modified activated alumina for fluoride removal from water. Journal of Hazardous Materials 278. 343–349.

Jung-Seok Yang, Young-Soo Kim, Sang-Min Park & Kitae Baek. (2014). Removal of As(III) and As(V) using iron-rich sludge produced from coal mine drainage treatment plant. Environmental Science and Pollution Research, 21:10878–10889

K.S.W. Sing, D.H. Everett, R.A.W. Haul, L. Moscou, R. A Pierotti, J. Rouquerol, T. Siemieniewska, (1985). Reporting physisorption data for gas/solid systems with special reference to the determination of surface area and porosity (Recommendations 1984), Pure Appl. Chem. 57 603–619.

Kenneth S.W. Sing and Ruth T. Williams. (2004). Physisorption Hysteresis Loops and the Characterization of Nanoporous Materials. Adsorption Science & Technology Vol. 22 No. 10.

Komorowicz, I. & Barałkiewicz, D. (2016). Determination of total arsenic and arsenic species in drinking water, surface water, wastewater, and snow from Wielkopolska, Kujawy-Pomerania, and Lower Silesia provinces, Poland. Environmental Monitoring and Assessment, 188: 504.

Langmuir, I. (1916). The constitution and fundamental properties of solids and liquids. Journal of the American Chemical Society, 38, 2221–2295.

Li, W., Cao, C. Y., Wu, L. Y., Ge, M. F., & Song, W. G. (2011). Superb fluoride and arsenic removal performance of highly ordered mesoporous aluminas. Journal of hazardous materials, 198, 143-150.

Long Liang, Liguang Wang, Anh V. Nguyen, Guangyuan Xie. (2017). Heterocoagulation of alumina and quartz studied by zeta potential distribution and particle size distribution measurements. Powder Technology 309, 1–12.

Majumder, C. (2018). Arsenic (V) Removal Using Activated Alumina: Kinetics and Modeling by Response Surface. Journal of Environmental Engineering, 144(3), 04017115.

Marshahida mat yashim and Erma liana marjohan. (2016). Adsorption isotherm study of adsorption methylene blue onto oil palm kernel shell activated carbon. Journal of Engineering and Applied Sciences, Vol. 11, 20.

Mohan Dinesh, Pittman Jr. Charles U. (2007). Arsenic removal from water/wastewater using adsorbents—A critical review. Journal of Hazardous Materials, 142, 1–53.

N. Inchaurrondo, C. di Luca, F. Mori, A. Pintar, G. Žerjav, M. Valiente, C. Palet. (2019). Synthesis and adsorption behavior of mesoporous alumina and Fe-doped alumina for the

removal of dominant arsenic species in contaminated waters. Journal Environmental Chemical Engineering, 7, 1, 102901.

Nicomel, N. R., Leus, K., Folens, K., Voort, P. V. D., and Laing, G. D. (2015). Technologies for Arsenic Removal from Water: Current Status and Future Perspectives. International Journal of Environmental Research and Public Health. 13: 62.

Pio, I., Scarlino, A., Bloise, E., Mele, G., Santoro, O., Pastore, T., and Santoro, D. (2015). Efficient removal of low-arsenic concentrations from drinking water by combined coagulation and adsorption processes. Separation and Purification Technology, 147: 284-291.

Pradnya Pillewan, Shrabanti Mukherjee, Tarit Roychowdhury, Sera Das, Amit Bansiwal, Sadhana Rayalu. (2011). Removal of As(III) and As(V) from water by copper oxide incorporated mesoporous alumina. Journal of Hazardous Materials, 186, 367–375

Renuka, N. K., Shijina, A. V., & Praveen, A. K. (2012). Mesoporous γ-alumina nanoparticles: synthesis, characterization and dye removal efficiency. Materials letters, 82, 42-44.

Roberto Leyva-Ramos, Nahum A. Medellín-Castillo, Araceli Jacobo-Azuara, Jovita Mendoza-Barrón, Lilia E. Landín-Rodríguez, José M. Martínez-Rosales and Antonio Aragón-Piña. (2008). Fluoride removal from water solution by adsorption on activated alumina prepared from pseudo-boehmite. Journal of Environmental Engineering and Management, 18(5), 301-309.

Saha, S., & Sarkar, P. (2012). Arsenic remediation from drinking water by synthesized nano-alumina dispersed in chitosan-grafted polyacrylamide. Journal of hazardous materials, 227, 68-78.

Sarkar, A., & Paul, B. (2016). The global menace of arsenic and its conventional remediation-A critical review. Chemosphere, 158, 37-49.

Shankar, S., Shanker, U., and Shikha (2014). Contaminación por arsénico del agua subterránea: una revisión de las fuentes, la prevalencia, los riesgos para la salud y las estrategias para la mitigación. The Scientific World Journal, 18.

Smedley PL, Kinniburgh DG (2002) A review of the source, behaviour and distribution of arsenic in natural waters. Applied Geochemistry, 17(5), 517–568.

Song, W., Zhang, M., Liang, J., & Han, G. (2015). Removal of As (V) from wastewater by chemically modified biomass. Journal of Molecular Liquids, 206, 262-267.

Sreejesh Nair, Lotfollah Karimzadeh, Broder J. Merkel (2014). Sorption of uranyl and arsenate on SiO_2, Al_2O_3, TiO_2 and FeOOH. Environmental Earth Science, 72:3507–3512

Taseidifar, M., Makavipour, F., Pashley, R. M., Mokhlesur-Rahman, A. F. M. (2017). Removal of heavy metal ions from water using ion flotation. Environmental Technology & Innovation, 8: 182-190

Vieira, B. R., Pintor, A. M., Boaventura, R. A., Botelho, C. M., and Santos, S. C. (2017). Arsenic removal from water using iron-coated seaweeds. Journal of Environmental Management, 192: 224-233.

Xunjun Chen. (2015). Modeling of Experimental Adsorption Isotherm Data. Information, 6, 14-22.

Yazdani, M. R., Tuutijärvi, T., Bhatnagar, A., & Vahala, R. (2016). Adsorptive removal of arsenic (V) from aqueous phase by feldspars: Kinetics, mechanism, and thermodynamic aspects of adsorption. Journal of Molecular Liquids, 214, 149-156.

Yin, H., Kong, M., Gu, X., and Chen, H. (2017). Removal of arsenic from water by porous charred granulated attapulgite-supported hydrated iron oxide in bath and column modes. Journal of Cleaner Production, 166: 88-97.

Younghun Kim, Changmook Kim, Inhee Choi, Selvaraj Rengaraj, and Jongheop Yi. (2004). Arsenic Removal Using Mesoporous Alumina Prepared via a Templating Method. Environmental Science & Technology, 38 (3), 924–931).

Yuan Ma, Qinglian Wei, Ruowen Ling, Fengkai An, Guangyu Mu, Yongmin Huang. (2013). Synthesis of macro-mesoporous alumina with yeast cell as bio-template. Microporous and Mesoporous Materials, 165, 177-184.

Yuh-Shan Ho. (2006). Review of second-order models for adsorption systems. Journal of Hazardous Materials B136, 681–689.

Zamorategui M., A., Ramírez R., N., Martínez R., J. M., & Serafín M., A. H. (2016). Synthesis and characterization of gamma alumina and compared with an activated charcoal on the fluoride removal from potable well water. Acta Universitaria, 26(2), 30-35.

Zhang, L., Wu, Y., Zhang, L., Wang, Y., & Li, M. (2016). Synthesis and characterization of mesoporous alumina with high specific area via coprecipitation method. Vacuum, 133, 1-6.